Analysis of Injection-Induced Micro-Earthquakes in a Geothermal Steam Reservoir, The Geysers Geothermal Field, California

Rutqvist, J. and Oldenburg C. M.

Earth Sciences Division, Lawrence Berkeley National Laboratory, Berkeley, California, USA

ABSTRACT: In this study we analyze relative contributions to the cause and mechanism of injection-induced micro-earthquakes (MEQs) at The Geysers geothermal field, California. We estimated the potential for inducing seismicity by coupled thermal-hydrological-mechanical analysis of the geothermal steam production and cold water injection to calculate changes in stress (in time and space) and investigated if those changes could induce a rock mechanical failure and associated MEQs. An important aspect of the analysis is the concept of a rock mass that is critically stressed for shear failure. This means that shear stress in the region is near the rock-mass frictional strength, and therefore very small perturbations of the stress field can trigger an MEQ. Our analysis shows that the most important cause for injection-induced MEQs at The Geysers is cooling and associated thermal-elastic shrinkage of the rock around the injected fluid that changes the stress state in such a way that mechanical failure and seismicity can be induced. Specifically, the cooling shrinkage results in unloading and associated loss of shear strength in critically shear-stressed fractures, which are then reactivated. Thus, our analysis shows that cooling-induced shear slip along fractures is the dominant mechanism of injection-induced MEQs at The Geysers.

1. INTRODUCTION

The Geysers is the site of the largest geothermal electricity generating operation in the world and is also one of the most seismically active regions in northern California [1]. It is a vapor dominated geothermal reservoir system, which is hydraulically confined by low permeability rock units. As a result of high rate of steam withdrawal, the reservoir pressure declined until the mid 1990s, when increasing water injection rates resulted in a stabilization of the steam reservoir pressure. If The Geysers were produced without simultaneously injecting water, reservoir pressures and flow rates from production wells would decline fairly rapidly to uneconomical levels. However, the water injection has also resulted in an increased level of seismicity at The Geysers, which has raised concerns regarding the social, environmental, and economic impacts on the local communities [1]. For public acceptance, a good understanding of the causes and mechanisms of induced seisimicity is important and may pave the way for finding ways to minimize the level of seismicity while optimizing energy production.

Over the past 25 years, a number of studies have been made to investigate the correlation between operational data and seismicity at The Geysers [1–9]. Perhaps the most comprehensive study in recent years was made by Mossop [8], who studied the correlation of induced seismicity and operational data from 1976 to 1998. Mossop [8] found three types of induced seismicity of high significance: i) Shallow, production-induced seismicity that has a long time lag, on the order of 1 year; ii) deep, injection-induced seismicity with short time lag, < 2 months; and iii) deep, production-induced seismicity with short time lag, < 2 months that appeared to diminish in the late 1980s. Injection-induced seismicity is typically clustered around injection wells, extending downward in plume-like forms Fig. 1 [9].

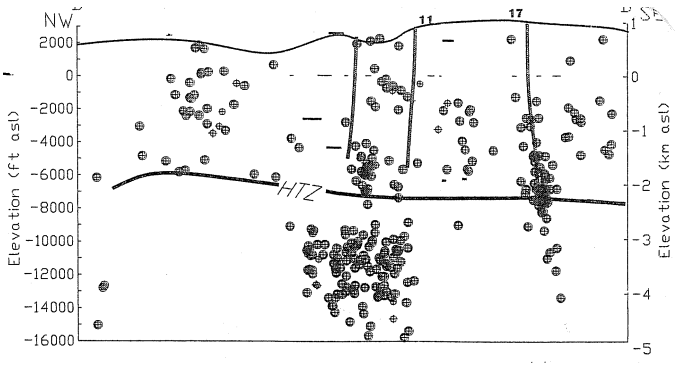

Fig. 1 NW-SE cross-section through The Geysers geothermal field showing 2002 MEQ hypocenters, injection wells, power plants, and top of the High Temperature Zone (HTZ) [9].

Several plausible hypotheses have been proposed to explain the cause and mechanism of producing MEQs at The Geysers. In is clear that the Geysers region is subject to active tectonic forces associated with the right-lateral strike-slip motion between the North-American and Pacific plates [9, 10]. Therefore, many naturally-occurring fractures may be stressed to near the failure point, so a small perturbation in the stress field could lead to failure. However, the exact causes and mechanisms of MEQs at The Geysers remain an area of active research.

In this paper we present results of a coupled thermal-hydrological-mechanical (THM) analysis to study the cause and mechanism for seismicity associated with energy extraction at The Geysers geothermal field. We conducted a coupled thermal-hydrological-mechanical numerical analysis of steam production and water injection and the causes and mechanisms of induced seismicity are determined by studying the evolution of the stress field (in time and space). Specifically, we investigated if production- and injection-induced changes in the stress field could induce a rock mechanical failure (such as shear failure along pre-existing fractures) which could give rise to seismicity.

2. MODEL SETUP

The coupled THM analysis was conducted with TOUGH-FLAC [11], a simulator based on linking the geothermal reservoir simulator TOUGH2 [12] with the geomechanical code FLAC3D. We conducted the simulations on a simplified two-dimensional model representing one-half of a NE-SW cross-section of the NW-SE trending Geysers geothermal field (Figure 1). Data from published papers [e.g 13] were used to constrain a conceptual model of the field, consisting of a low-permeability cap and a very-low-permeability lateral boundary that defined a reservoir approximately 10 km wide by 3 km deep (Figure 2). The equivalent fractured rock permeability in the reservoir is $1 \cdot 10^{-14}$ m^2 (10 millidarcy) with a 2% porosity. The grid, taking advantage of symmetry, models a 5 km wide section in the northeastern part of The Geysers. The initial (pre-production) conditions were established through a steady state multi-phase flow simulation. The initial reservoir temperature is about 240°C down to depth of 3.5 km and then gradually increases to 350°C towards the bottom boundary at a depth of 5.5 km. The initial steam pressure within the reservoir is about 4 MPa, whereas the pressure outside the sealed reservoir is hydrostatic.

The initial thermal and hydrogeological conditions mimics the general behavior of The Geysers and show (1) Typical Geysers Reservoir (TGR) above the (2) High-Temperature Reservoir (HTR), (3) cap hydraulically separate from reservoir, and (4) hydrostatic pressure and normal geothermal gradient at large lateral distance from the reservoir.

The THM analysis was conducted with a linear poroelastic model. A rock-mass bulk modulus of 3 GPa was adopted, which approximately corresponds to values back-calculated by Mossop and Segall [14] based on strain analyses at The Geysers. The rock thermal expansion coefficient was set to 3×10^{-5} $°C^{-1}$, which corresponds to values determined on core samples of the reservoir rock at high (250 °C) temperature [14]. Note that although we are using a two-dimensional plane strain model, we are able to calculate changes in the three-dimensional stress field, including stresses within the x-z plane as well as out-of-plane stress (i.e., stress in the y-direction).

The coupled THM analysis of the potential causes and mechanisms of injection-induced seismicity were studied at two temporal scales:

1) Analysis of 44 years of production/injection from 1960 to 2004;
2) Analysis of seasonal injection cycles during 2005.

Steam was produced at the left-hand side (mirror plane) boundary of the two-dimensional Cartesian model between 1,600 to 3,000 m depth, and water was injected at a distance of 217 m from the left boundary of the model, also between 1,600 to 3,000 m depth. The steam production and injection rates were derived from field-wide data at The Geysers from 1960 through 2005 shown in Figure 3. For our two-dimensional (1 meter thick) simulation model, the field-wide production/injection rates were reduced to approximately 5×10^{-5} times the values shown in Figure 3. This reduction arises from geometric considerations such as the difference in width of the model and the actual system. Specifically, the Geysers field is 13 km long while our two-dimensional Geysers model is 1 m wide. This difference corresponds to a factor of 1.3×10^4 reduction in production and injection rates relative to the actual Geysers field. The remaining reduction by a factor of approximately 1.5 can be explained by the fact that we are modeling a two-dimensional slice as opposed to a radial system, which would allow for radial in/out flow. For the production well, the rate was further halved to correspond to a mirror plane in the conceptual model of the system. For the analysis of 44 years production/injection, yearly average values were used, whereas monthly values were used for the analysis of seasonal injection cycles. We emphasize that the two-dimensional cross-section model and the production and injection rates we are using are not meant to be a precise model of the Geysers system, but rather an analog model capable of representing fundamental processes of THM coupling.

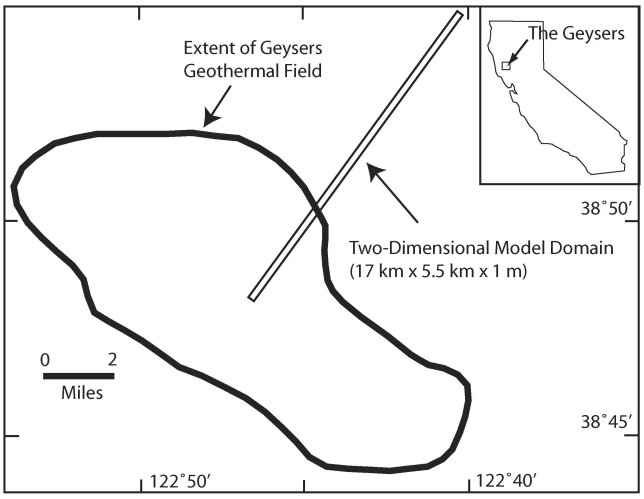

(a)

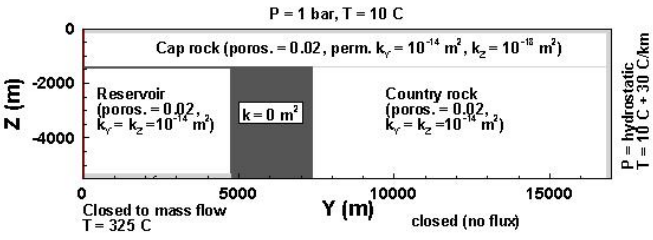

(b)

Fig. 2. Two-dimensional model for coupled THM analysis of induced seismicity at The Geysers. (a) Location map of The Geysers showing approximate boundary of the geothermal reservoir and orientation of the two-dimensional model domain and (b) model geometry with hydraulic properties of different rock units and boundary conditions.

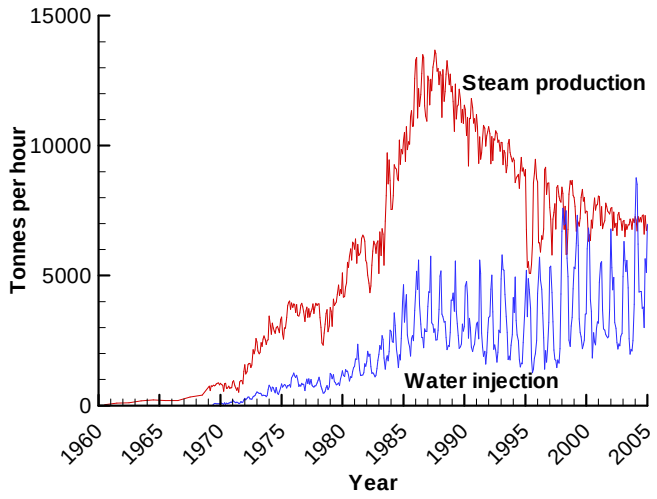

Fig. 3. The Geysers reservoir-wide steam-production and water-injection rates from 1960 to 2005 used as the basis for input to the coupled THM analysis (data also shown in Stark et al. [15] and were obtained from M. Stark of Calpine by personal communication).

3. APPROACH FOR FAILURE ANALYSIS

One of the main features of our mechanical model is the analysis of stress path and the potential for shear failure within a critically stressed rock mass (Fig. 4). The concept of a critically stressed rock mass at The Geysers arose from early rock-mechanical studies of Geysers samples that indicated that the rock has undergone extensive hydrothermal alterations and re-crystallization, and that it is highly fractured [16]. Lockner et al. [16] suggested that fracturing has weakened the rock to such an extent that models of the geothermal field should assume that only a frictional sliding load can be supported by the rock, and the authors maintained that shear stress in the region is probably near the rock-mass frictional strengths. Therefore very small perturbations of the stress field could trigger seismicity. Based on the concept of a critically stressed rock mass, one of the main mechanisms we investigate at The Geysers is shear failure along existing fractures caused by small stress-field perturbations.

For the failure analysis, we evaluated the potential for shear slip under the conservative assumption that fractures of any orientation could exist anywhere (Fig. 4a). Such assumptions were confirmed by studies of fault plane analysis by Oppenheimer [10], which indicated that seismic sources are located at almost random orientations relative to faults. One key parameter in estimating the potential for fault slip is the coefficient of static friction, μ, entering the Coulomb shear failure criterion. Cohesionless faults are usually assumed to have a friction coefficient of 0.6 to 0.85 (e.g. [17]). Moreover, a frictional coefficient of $\mu = 0.6$ is a lower-limit value observed in fractured rock masses [17]. Thus, using $\mu = 0.6$ in the Coulomb criterion would most likely give a conservative estimate of the potential for induced seismicity. For $\mu = 0.6$, the Coulomb criterion for the onset of shear failure can be written in the following form:

$$\sigma'_{1c} = 3\sigma'_3 \qquad (1)$$

where σ'_{1c} is the critical maximum principal stress for the onset of shear failure. Thus, shear slip (and induced seismicity) would be induced whenever the change in maximum principal effective stress exceeds three times the change in minimum principal stress. However, based on the concept of a critically stressed rock mass, we assume that the initial stress is in a state of incipient failure, i.e., located on the failure envelope $\sigma'_1 = 3\times\sigma'_3$, and investigate whether the stress state tends to move away from or towards a state of failure (Fig. 4b, c and d). The state of stress would move towards failure if the change in maximum principal compressive effective stress exceeds three times the change in minimum principal effective stress (i.e., if $\Delta\sigma'_1 \geq 3\times\Delta\sigma'_3$, failure is likely). Conversely, the state of stress would move away

from failure if the change in maximum principal compressive effective stress is less than three times the change in minimum principal effective stress (i.e., if $\Delta\sigma'_1 < 3\times\Delta\sigma'_3$, failure is unlikely). Moreover, we investigate the potential for failure defined by comparing the current change in maximum principal stress to the critical change in maximum principal stress for the onset of failure, i.e., $\Delta\sigma'_{1m} = \Delta\sigma'_1 - \Delta\sigma'_{1c} = \Delta\sigma'_1 - 3\times\Delta\sigma'_3$. If the current stress change $\Delta\sigma'_1$ exceeds the critical change $\Delta\sigma'_{1c}$, the quantity $\Delta\sigma'_{1m}$ becomes negative indicating that the stress state has moved into a state of failure.

The path of stress changes, including whether the minimum or maximum principal stresses will increase or decrease, can be calculated with much more certainty than the magnitude of stress changes. The magnitude of stress changes resulting from temperature and fluid pressure changes depends on a number of mechanical properties, such as elastic modulus and thermal expansion coefficient, whereas the direction of stress changes (e.g., increase or decrease) is much less dependent on the exact values of mechanical properties.

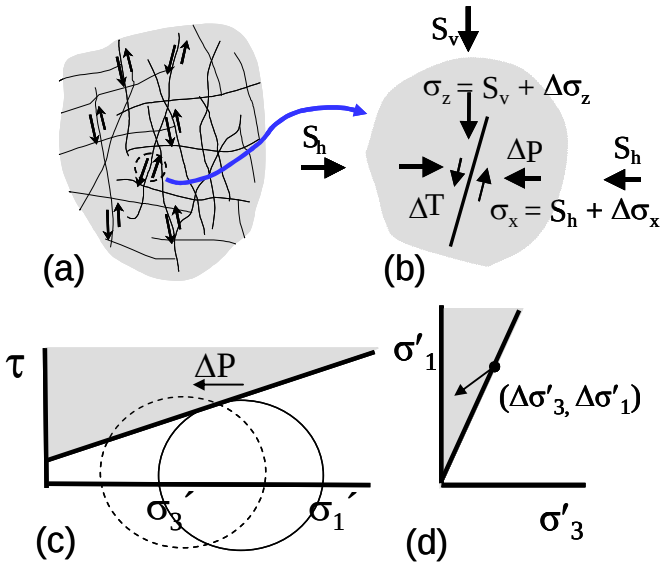

Fig. 4. Illustration of the approach for failure analysis to evaluate the potential for induced seismicity at The Geysers (a) Highly fractured rock with randomly oriented fractures, (b) Changes in stress on one fracture plane, (c) Movements of Mohr's circle as a results of increased fluid pressure within a fracture plane for a critically stressed fracture, and (d) corresponding stress path in the (σ'_1, σ'_3) plane.

4. ANALYSIS OF 44 YEARS OF PRODUCTION/INJECTION

The simulation of 44 years of steam-production and injection resulted in a reservoir-wide pressure and temperature decline of a few MPa and a few degrees, respectively, as well as subsidence of about 0.5 to 1 meter. These numbers are in general agreement with field observations at the Geysers [14]. This provides evidence that the adopted rock-mass bulk modulus of 3 GPa and the thermal expansion coefficient of to 3×10^{-5} °C^{-1} are reasonably accurate and that the calculated basic THM responses of the reservoir are reasonable.

Figure 5 shows calculated liquid saturation and changes in fluid pressure and temperature after 44 years of production/injection. Figure 5a shows that the injection caused formation of a wet zone that extends downwards 1,000 m and all the way to the production well. Figure 5c indicates a local cooling effect wherever the water flows, especially where the liquid reaches the production well. The injection has a significant effect on the fluid pressure at depths towards the bottom of the model, where pressure depletion is prevented (Figure 5b).

Figures 6a and b depict changes in vertical and horizontal effective stresses, respectively. The stress change in the rock mass is caused by both production-induced depletion and injection-induced cooling. The depletion and cooling cause a general shrinkage of the reservoir, which in turn gives rise to increased horizontal stresses near the ground surface (Figure 6a). The main effect of water injection is a reduction of vertical effective stress within the zone of cooling. The cooling shrinkage near the wells is stronger in the vertical direction because the zone of cooling is elongated vertically.

Figure 6c shows the calculated distribution of failure potential, which is represented by the parameter $\Delta\sigma'_{1m} = \Delta\sigma'_1 - \Delta\sigma'_{1c}$ described above. In Figure 6c, red and yellow colors show the zones that are most prone to failure, whereas blue color shows the zones that are least prone to failure. The figure indicates that failure (and induced seismicity) caused by production/injection would occur both near the ground surface and close to the wells, and at depth below the wells (Figure 6c).

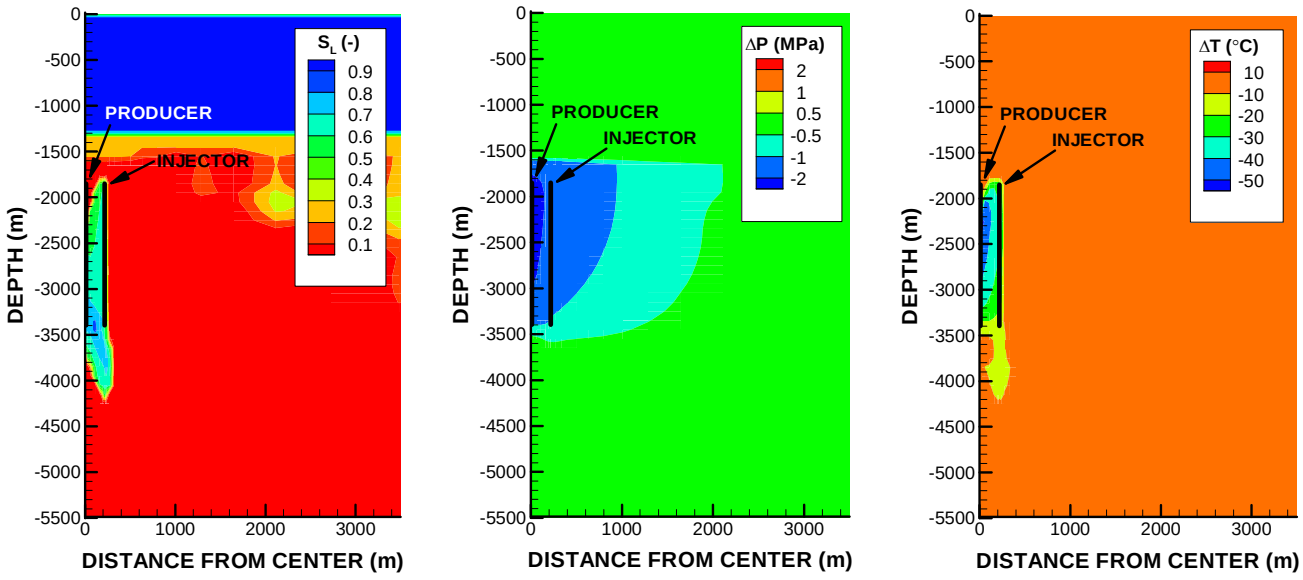

Fig. 5. Calculated basic thermal-hydrological responses after 44 years of production/injection. (a) liquid saturation, (b) change in fluid pressure, and (c) change in temperature.

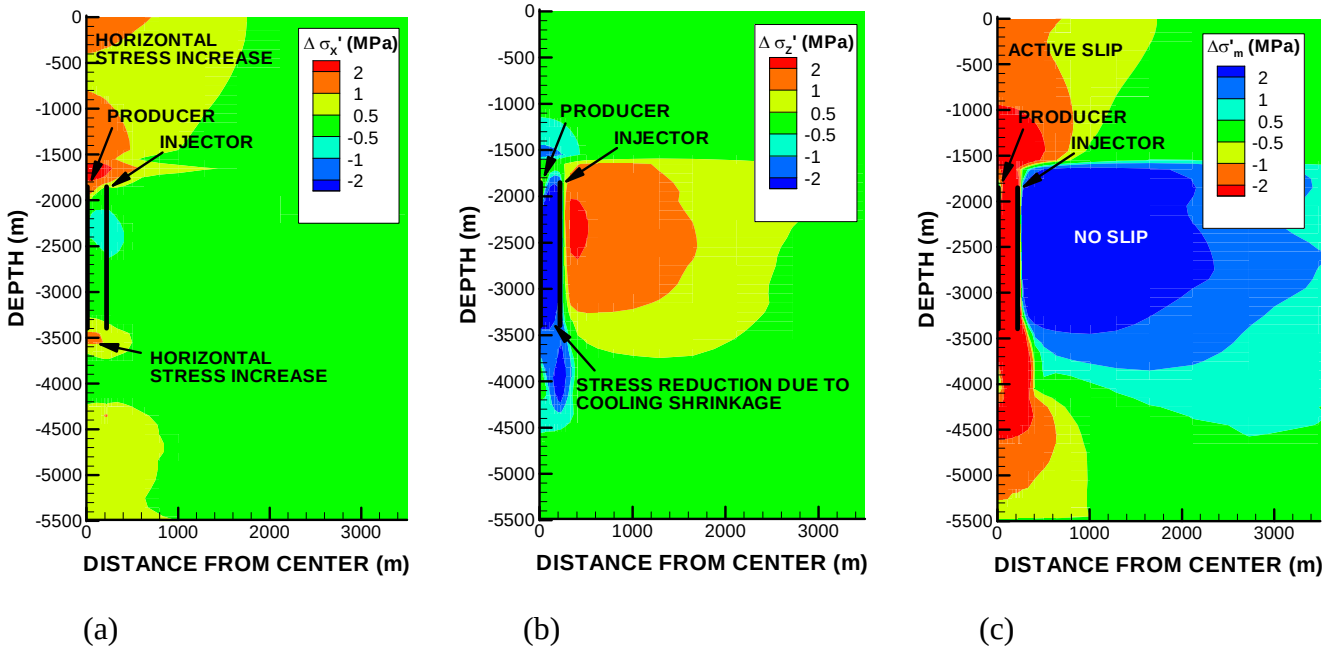

Fig. 6. Calculated geomechanical responses after 44 years of production/injection. Changes in (a) horizontal effective stress (b) vertical effective stress and (c) potential for failure, $\Delta\sigma'_{1m} = \Delta\sigma'_1 - \Delta\sigma'_{1c}$.

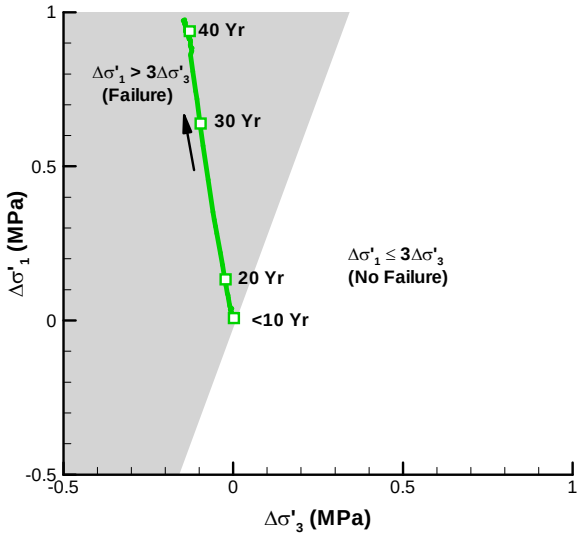

(a)

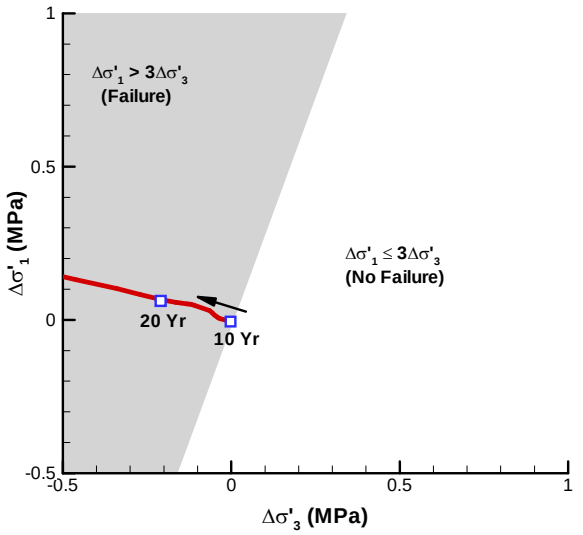

(b)

Fig. 7. Calculated path of changes in the stress state (σ'_1, σ'_3) monitored (a) within the caprock at (x = 0, z = -750 m) and (b) within the reservoir at the bottom of the injection well (x = 217.5 m, z = -3325 m).

Figures 7 depict the stress path for two points near the central part of the geothermal field. The stress path is compared to the failure envelope ($\Delta\sigma'_1 = 3\times\Delta\sigma'_3$) for the likely scenario of maximum compressive *in situ* stress being horizontal. In the caprock at a depth of about 750 m (Figure 7a), there is a slow monotonic increase in maximum principal stress. This stress increase is a reaction to poroelastic and thermal shrinkage within the underlying steam reservoir, which in turn is caused by the reservoir-wide pressure and temperature decline. At the bottom of the injection well the stresses are driven into failure as a result of local cooling of the rock which tends to reduce the minimum principal effective stress.

5. ANALYSIS OF SEASONAL INJECTION CYCLES

We analyzed the effects of seasonal injection cycles corresponding to 2005 production/injection rates. Our initial conditions are those achieved at the end of the 44-year simulation period, from 1960 to 2004. Thus, in this case we study mechanical changes that occur during 12 months with respect to the mechanical state at the end of December 2004.

Figure 8 presents the basic thermal-hydrological responses, i.e., liquid saturation, and changes in fluid pressure and temperature after 6 months. The seasonal injection, which peaks at about 1 to 2 months, produces a pulse of liquid flow that travels along the existing wet zone, towards the production well and downwards about 1,000 m below the wells. For example, comparing Figure 8a with Figure 5a we can see some increased liquid saturation within the wet zone. This pulse causes a pressure increase and cooling near the bottom of the wet zone when the liquid water hits dryer and hotter rocks (Figure 8b and c).

Figure 9 shows the calculated distributions of stress changes and failure. Zones of high potential for failure occur along the injection borehole and around the zone of cooling and elevated fluid pressure at the bottom of the wet zone, i.e., about 1,000 m below the injection well. Along the borehole, the zone of failure (Figure 9c) correlates with the zone of cooling (Figure 9c) and reduced vertical effective stress (Figure 9b). The failure zone located 1,000 m below the injection well (Figure 9c) correlates with the zone of cooling (Figure 8c) and the zone of reduced effective stresses (Figure 9a and b). The mechanism of failure (and induced seismicity) is shear reactivation of fractures caused by a reduction in frictional strength as effective stresses are reduced, which in turn is caused by cooling shrinkage, and to a smaller extent by elevated fluid pressure at depths.

Figure 10 compares the time evolution of injection rate and potential for failure ($\Delta\sigma'_m = \Delta\sigma'_1 - \Delta\sigma'_{1c}$). Overall, the simulation results indicate that near the injection well there is a time lag of a few months (Figure 10a), which is related to the time it takes for the injected cold water to induce local rock cooling. At 5,000 m depth, the longer time lag is related to the time it takes for the fluid pressure to propagate downwards and reduce the effective stresses (Figure 10b).

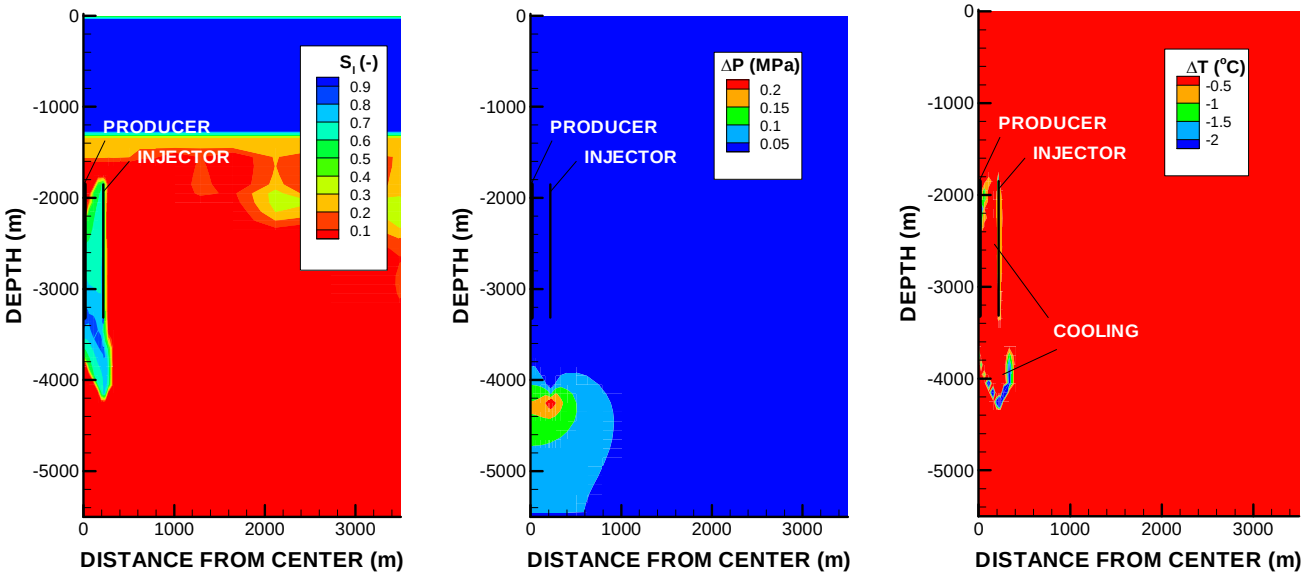

(a) (b) (c)

Fig. 8. Calculated basic thermal-hydrological responses after 6 months of the 2005 seasonal injection analysis. (a) liquid saturation, (b) changes in fluid pressure, and (c) changes in temperature.

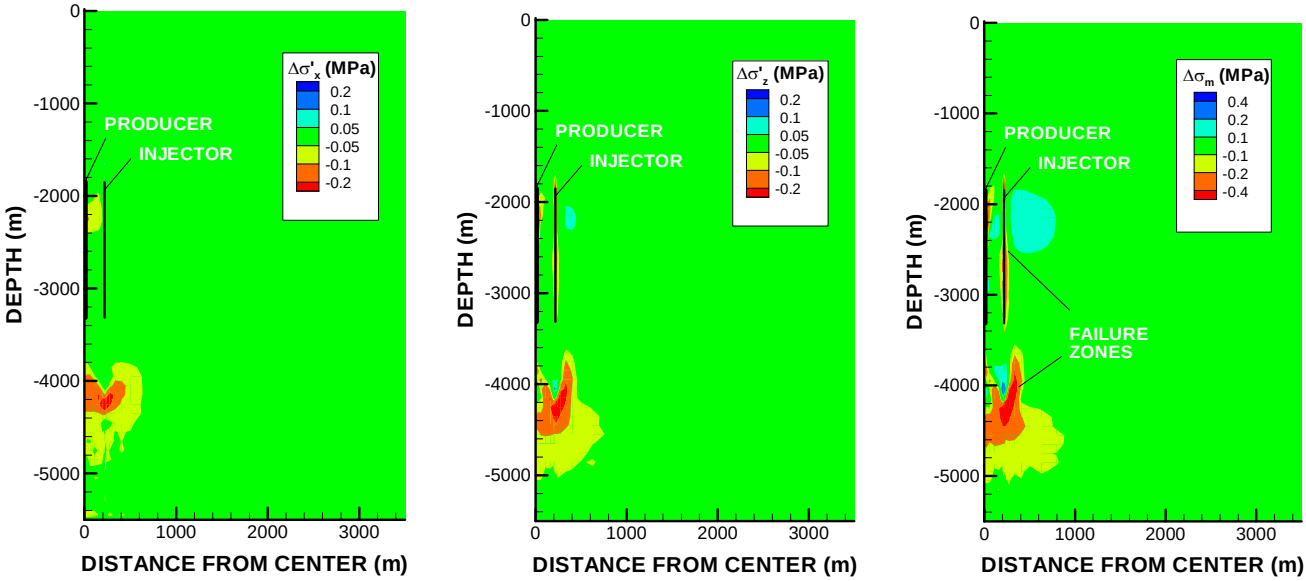

(a) (b) (c)

Fig. 9. Calculated geomechanical responses after 6 months of the 2005 seasonal injection. Changes in (a) horizontal effective stress (b) vertical effective stress and (c) potential for failure, $\Delta\sigma'_{1m} = \Delta\sigma'_1 - \Delta\sigma'_{1c}$.

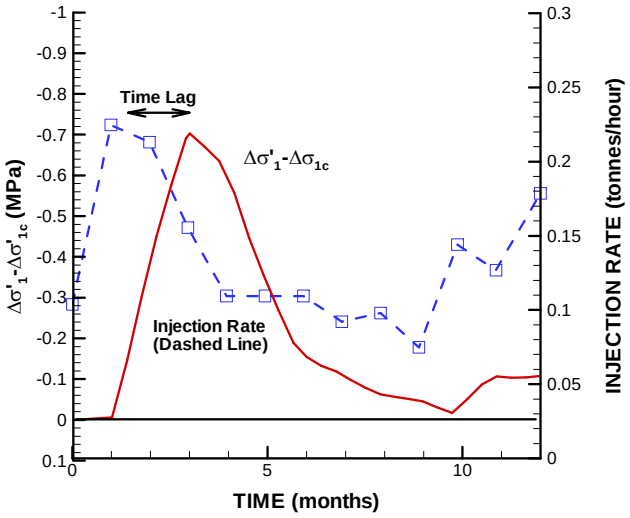

(a)

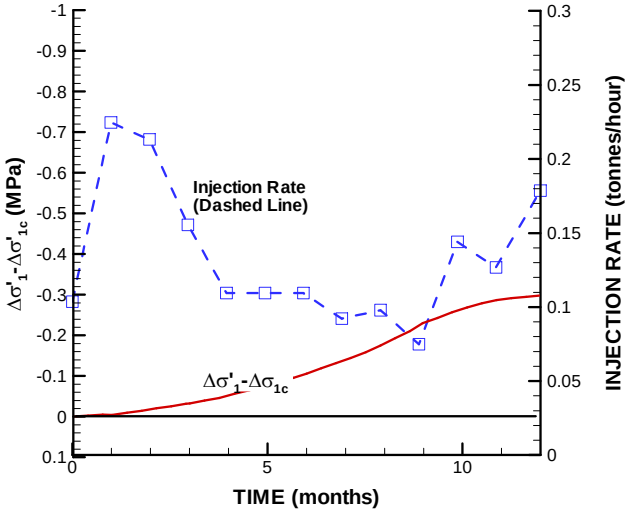

(b)

Figure 10. Comparison of injection rate and evolution of failure margin ($\Delta\sigma'_1$ - $\Delta\sigma'_{1c}$) at (a) the bottom of the injection well (x = 217.5 m, z = -3325 m), and at (b) about 1700 m below the injection well (x = 217.5 m, z = -5000 m).

6. CONCLUSIONS

We analyzed the cause and mechanism of induced seismicity at The Geysers geothermal field, California, using coupled thermal-hydrological-mechanical numerical modeling. Our results are in qualitative agreement with field observations (e.g., [9]). Specifically, both modeling and field observations show that most of the injection-induced seismicity occurs near injection and production wells, and can spread several kilometers below injection wells (compare Figure 1 and 9c). Moreover, the analysis shows a typical time lag between seasonal peak injection rates and peaks in induced seismicity. Based on our analysis, we draw the following specific conclusions regarding relative contributions to the cause and mechanism of induced seismicity at The Geysers:

- Shear slip along existing fractures as a result of reduced minimum principal compressive stress is the most likely mechanism of induced-seismicity at The Geysers.
- Near injection and production wells, thermal-elastic cooling shrinkage is the dominant cause for stress changes leading to injection-induced seismicity.
- At greater depths below production and injection wells, both thermal-elastic cooling shrinkage and increased fluid pressure as a result of injection may contribute to reducing effective stress leading to deep injection-induced seismicity.
- Injection-induced seismicity could also occur in the shallow parts of the system and in the cap rock caused by stress redistribution from injection-induced cooling shrinkage within the underlying reservoir.

Future modeling will include injection into a discrete high permeable vertical fracture, which could explain fast propagation and short time lag between injection and seismicity located far below the injection wells as observed by Stark [9].

ACKNOWLEDGMENTS

This work was conducted with funding from the California Energy Commission (CEC) with matching funds from the Assistant Secretary for Energy Efficiency and Renewable Energy, Geothermal Technologies Program, of the U.S. Department of Energy under Contract No. DE-AC02-05CH1123

REFERENCES

1. Majer, E.L. and J.E. Peterson. 2007. The impact of injection on seismicity at The Geysers, California Geothermal Field. *Geothermics.* 44:1079–1090.
2. Majer, E.L., and T.V. McEvilly. 1979. Seismological investigations at the Geysers Geothermal Field, *Geophysics*, 44:246–269.
3. Eberhart-Phillips, D and D.H. Oppenheimer. 1984. Induced seismicity in The Geysers Geothermal Area, California, *J. Geophys. Res.*, 89:1191–1207.
4. Enedy, S.L., K.L. Enedy, and J. Maney. 1992. In Monograph on the Geyser geothermal field, Special report no. 17, Geothermal Research Council, pp. 211-218.
5. Stark, M.A. 1992. Microearthquakes – a tool to track injected water in The Geysers reservoir. In Monograph on the Geyser geothermal field, Special report no. 17, Geothermal Research Council, pp. 111-117.
6. Kirkpatrick, A., J.E. Peterson, E.L. Majer and R Nadeau. 1999. Characteristics of microseismicity in the DV11 injection area, Southeast Geysers, California. Proc. 24th Workshop on Geothermal Reservoir Engineering, Stanford, California, January 25–27, 1999.
7. Smith, J.L.B, J.J. Beall and M.A. Stark .2000. Induced seismicity in the SE Geysers Field. *Geotherm. Resourc. Counc. Trans.* 24, 24–27.
8. Mossop, A.P. 2001. Seismicity, subsidence and strain at The Geysers geothermal field. Ph.D. dissertation, Stanford University.
9. Stark, M.A. 2003. Seismic evidence for a long-lived enhanced geothermal system (EGS) in the Northern Geysers Reservoir, *Geothermal Resourc. Counc. Transactions*, 27, 727-731.
10. Oppenheimer, D.C. 1986. Extensional tectonics at the Geysers Geothermal Area, California, J. Geophys. Res., 91, 11463–11476.
11. Rutqvist, J., Y.-S. Wu, C.-F. Tsang and G. Bodvarsson. 2002. A Modeling Approach for Analysis of Coupled Multiphase Fluid Flow, Heat Transfer, and Deformation in Fractured Porous Rock. *Int. J. Rock mech. Min. Sci*. 39, 429-442.
12. Pruess, K., Oldenburg, C.M., and Moridis, G.M., TOUGH2 User's Guide Version 2. E. O. Lawrence Berkeley National Laboratory Report LBNL-43134, November 1999.
13. Williamson, K.H. 1992. Development of a reservoir model for the Geysers Geothermal Field, Monograph on The Geysers Geothermal Field, Geothermal Resources Council, Special Report no. 17, 179-18.
14. Mossop, A.P. and P. Segall, P. 1997. Subsidence at The Geysers geothermal field, N. California from a comparison of GPS and leveling surveys. Geophys. Res. Letter 24, 1839–1842.
15. Stark, M.A., W.T. Box, J.J. Beall, K.P. Goyal and A.S. Pingol. 2005. The Santa Rosa-Geysers recharge project, Geysers Geothermal Field, California, GRC Transactions, 29, 145-150.
16. Lockner, D.A., R. Summer, D. Moore and J.D. Byerlee. 1982. Laboratory measurements of reservoir rock from the Geysers Geothermal Field, California. *Int. J. Rock mech. Min. Sci*. 19, 65-80.
17. Barton, C.A.. M.D. Zoback and D. Moos. 1995. Fluid flow along potentially active faults in crystalline rock. *Geology*, 23:683–686.